

Sigmoid generalized complementary equation for evaporation over wet surfaces: A nonlinear modification of the Priestley–Taylor equation

Songjun Han¹, Fuqiang Tian², Wei Wang³, Liming Wang²

Key Points:

- Sigmoid generalized complementary (SGC) equation is applied to wet surfaces
- Wet surface SGC equation outperforms the linear Priestley–Taylor (PT) equation because it considers the varying PT coefficient
- Complementary principle can be extended to include advections or large-scale synoptic changes

Abstract: The deviations of the Priestley–Taylor (PT) coefficient from a fixed value around 1.26 indicate a nonlinear dependence of wet surface evaporation (E) on the equilibrium evaporation (E_{rad} , which is the radiation term in Penman potential evaporation (E_{pen})). The linear PT equation with a fixed coefficient underestimates E for small E_{rad} but overestimates E for large E_{rad} . In this study, the sigmoid generalized complementary (SGC) equation by Han and Tian (2018) was applied to estimate the wet surface evaporation by setting its asymmetric parameter to infinity. The SGC equation with one fixed parameter captures the nonlinear dependence of E on E_{rad} over the wet surface by including the aerodynamic component of E_{pen} , and amends the shortage of the linear PT equation. By using datasets over open water surfaces of lakes and ocean, wetlands, and paddy fields, the validation results indicate that the wet surface SGC equation performed better than the linear PT equation on evaporation estimation, especially over open water surfaces, where advections or large-scale synoptic changes are more substantial. The success of the wet surface SGC equation has implications for the extension of the complementary principle to consider above processes.

Key words: Evaporation; wet surface; complementary principle; Priestley–Taylor equation

1 Introduction

The evaporation over a landscape where the water supply is unlimited (defined as wet surface hereafter), such as open water, wetlands, and paddy fields, etc., is governed by the available energy and atmospheric conditions (Granger, 1989; Katul & Parlange, 1992). Wet surface evaporation is sensitive to climate change and it is crucial to understand its processes for the studies of the hydrological response to climate change (Brutsaert & Parlange, 1998; Friedrich et al., 2018; Roderick & Farquhar, 2002; Wang et al., 2018a; Wang et al., 2018b). In addition, wet surface evaporation is the basis of the concept of potential evaporation (Penman, 1948; Priestley & Taylor, 1972). Quantifying wet surface evaporation is important as a reference potential evaporation for estimating actual evaporation from unsaturated surface (Allen et al., 1998; Bouchet, 1963; Budyko, 1974; McMahon et al., 2013).

Energy supply and mass transfer mechanism are required for estimating wet surface evaporation (Brutsaert, 2005). The methods for estimating wet surface evaporation can be categorized into several groups, including the energy budget, aerodynamic, and their combination, except for empirical approaches (Winter et al., 1995). Penman (1948) first combined the energy budget and mass transfer equation for open water evaporation, which is expressed as

$$E_{Pen} = \frac{\Delta}{\Delta + \gamma} (R_n - R_{es}) + \frac{\gamma}{\Delta + \gamma} f(u)(e^* - e_a), \quad (1)$$

where Δ is the slope of saturation vapor curve at air temperature, γ is a psychrometric constant, R_n is the net radiation, R_{es} is the residual of energy balance, including ground heat flux, heat stored in the water, and net heat flux carried by water flow etc., e_a is the vapor pressure at the reference height, e^* is the saturation vapor pressure, and $f(u)$ is a function of wind speed. The two terms on the right-hand side of Equation (1) are commonly referred to as radiation (E_{rad}) and aerodynamic (E_{aero}) terms.

Over an extensive wet surface under well-established steady conditions where the air tends to be saturated, evaporation would proceed at E_{rad} , and it is considered an equilibrium evaporation (Slatyer & McIlroy, 1961). The atmosphere above a wet surface always tends to depart from the equilibrium state because the regional or large-scale advection affects horizontal surface variation or atmospheric conditions (Brutsaert & Stricker, 1979). Thus, the true equilibrium conditions rarely occur, and the vapor pressure deficit is maintained because some degrees of advection always exist. Priestley and Taylor (1972) proposed an empirical equation based on equilibrium evaporation

E_{rad} for wet surface evaporation under an assumption of minimum advection (termed as “advection-free” by Priestley and Taylor (1972)).

$$E_{PT} = \alpha_{PT} E_{rad}, \quad (2)$$

where α_{PT} is the Priestley–Taylor (hereafter referred to as PT) coefficient to account for the advection. Although α_{PT} varies with the environment (Assouline et al., 2016; Eagleson, 2002), it is widely accepted to be in the range of 1.20–1.30 (Brutsaert, 2005) and is used as a constant with a best estimate of 1.26 (Brutsaert & Stricker, 1979; Priestley & Taylor, 1972). In this study, we use α_{PT}^c to denote the fixed and constant PT coefficient to avoid confusion.

E_{Pen} and E_{PT} were widely used for estimating wet surface evaporation (McMahon et al., 2013; Winter et al., 1995; Zhao & Gao, 2019) and were combined by De Bruin (1978) to estimate lake evaporation for eliminating the energy term. Although the aerodynamic term E_{aero} is not included in Equation (2), it was thought to account for a fixed proportion of the evaporation rate and was widely used to explain the variations of E_{PT} by supposing $E_{Pen} = E_{PT}$ over an extensive wet surface (Brutsaert, 1982; Eagleson, 2002; Priestley & Taylor, 1972). This assumption was immediately adopted by the complementary principle in the manner of the advection–aridity (AA) approach (Brutsaert, 2015; Brutsaert & Stricker, 1979), where E_{Pen} and E were hypothesized to merge to E_{PT} with increasing water availability of the land surface. Thus, E_{PT} was treated as a limit on E , $E \leq E_{PT} \leq E_{Pen}$, and a fixed PT coefficient α_{PT}^c was usually used in practice (Brutsaert, 2015; Brutsaert & Stricker, 1979). On the basis of this wet boundary condition, a linear complementary relationship was derived for evaporation over a natural surface (Brutsaert & Parlange, 1998; Brutsaert & Stricker, 1979).

$$\frac{E}{E_{Pen}} = (1 + b^{-1}) \alpha_{PT}^c \frac{E_{rad}}{E_{Pen}} - b^{-1}, \quad (3)$$

where b is the asymmetry parameter and increases with the land surface wetness (Wang et al., 2020). By setting b approaching infinity, Equation (3) becomes

$$\frac{E}{E_{Pen}} = \alpha_{PT}^c \frac{E_{rad}}{E_{Pen}}, \quad (4)$$

which is identical to the linear PT Equation (2).

A major innovation of the PT equation is to eliminate the aerodynamic term with a fixed coefficient via the assumption of a linear relationship between E and E_{rad} (as well as $\frac{E}{E_{Pen}}$ and $\frac{E_{rad}}{E_{Pen}}$) over wet surfaces. Such a treatment is only strictly valid if the

aerodynamic control on wet surface evaporation is a fixed proportion of equilibrium evaporation E_{rad} , which may hold under the condition with a fixed advection effect. $\alpha_{PT}^c=1$ represents the condition without advection when the aerodynamic control vanishes (Slatyer & McIlroy, 1961), and $\alpha_{PT}^c=1.26$ represents the minimal advection condition where E_{aero} accounts for 26% of E_{rad} (Brutsaert, 1982). However, α_{PT} is enhanced by the horizontal advection of dry air mass (Jury & Tanner, 1975) or the vertical entrainment from above the planetary boundary layer (Baldocchi et al., 2016). It may also be affected by other processes, such as the behavior of the convective boundary layer, the dissimilarly in sources and sinks of heat and water vapor at the water surface (Assouline et al., 2016), and the large-scale synoptic changes (Guo et al., 2015; Liu et al., 2011). Under such conditions, α_{PT} is likely to be relatively different from 1.26 (Brutsaert & Stricker, 1979). Many studies have reported that α_{PT} shows large variations over wet surfaces (Assouline et al., 2016; Eagleson, 2002).

The variations of α_{PT} demonstrate a nonlinear dependence of E on E_{rad} over wet surfaces. The linear PT equation with a fixed coefficient $E = \alpha_{PT}^c E_{rad}$ is only an approximation. The accurate modeling of wet surface evaporation requires a consideration of the varying α_{PT} . Several methods were proposed to parameterized the varying α_{PT} by including the vapor pressure deficit and/or air temperature (Eichinger et al., 1996; Jury & Tanner, 1975), sensible heat flux (Parlange & Katul, 1992), relative transport efficiency of heat and water vapor (Assouline et al., 2016), and surface temperature (Yang & Roderick, 2019). However, the α_{PT} variations cannot be fully explained by using one variable (Assouline et al., 2016). One question then arises: is there any other method that can capture the wet surface evaporation and quantify its amount?

Han et al. (2012) and Han and Tian (2018a) derived a sigmoid generalized complementary equation (hereafter referred to as the SGC equation) as a nonlinear modification of the linear AA equation (3). Not involving the variations of α_{PT} in advance, the SGC equation expresses $\frac{E}{E_{Pen}}$ as a sigmoid function of $\frac{E_{rad}}{E_{Pen}}$, which appears as an S-shape curve in the state space $[\frac{E_{rad}}{E_{Pen}}, \frac{E}{E_{Pen}}]$. The parameters of the SGC equation can be determined from the parameters of the linear AA equation (PT coefficient and asymmetry parameter b) (Han & Tian, 2018a). The evaporation predicted by the SGC equation reaches E_{Pen} when $\frac{E_{rad}}{E_{Pen}}$ approaches its maximum

value, but approaches E_{PT} when asymmetry parameter $b \rightarrow \infty$. Thus, the SGC equation, which adopts a nonlinear relationship between $\frac{E}{E_{Pen}}$ and $\frac{E_{rad}}{E_{Pen}}$, shows a potential to amend the bias of the linear PT equation.

This study aims to apply the SGC equation for wet surface evaporation and explore its capacity as a nonlinear modification of the PT equation. Using the observed data of five lake sites from the Taihu Eddy Flux Network (Lee et al., 2014), a large shallow freshwater lake in southern China, we first investigate the nonlinear dependence of E on E_{rad} over the water surface of Lake Taihu to reveal the variations of the PT coefficient. Second, we examine the nonlinear dependence of $\frac{E}{E_{Pen}}$ on $\frac{E_{rad}}{E_{Pen}}$ over lake and ocean surfaces and demonstrate the ability to capture it by the SGC equation. We then validate the wet surface SGC equation for evaporation over open water surfaces of lakes and ocean, two wetlands and two paddy sites, with a comparison to the linear PT equation. Finally, we make some discussions on the capability of the wet surface SGC equation to capture the variations of PT coefficient, the effects of advections on its parameter, and new insights into the generalized complementary principle.

2 Wet surface SGC equation accounting for varying α_{PT}

2.1 Variation characteristics of α_{PT} synthesized from published papers

The published results were collated to investigate the variations of α_{PT} (Table 1). From the table, α_{PT} calculated by Equation (2) exhibits a large variation at the sub-daily timescale in the investigated studies. α_{PT} is 1.0–2.04 on a large shallow reservoir (Ross Barnett Reservoir) in Mississippi with a depth of approximately 4–8 m (Guo et al., 2015), 0.60–4.80 on the Tilopozo wetland of the Atacama Desert in Chile (Assouline et al., 2016), 0.67–3.12 on the moist tropical forest Amazon (Knox et al., 2016), and approximately 1.0–3.9 on an irrigated cropland site in North China Plain (Li & Yu, 2007). At the daily or monthly timescales, the variations in α_{PT} become weak but is still larger than the widely accepted range [1.2, 1.3]. Substantial variations of α_{PT} can also be found at the annual timescale. A reduction of annual α_{PT} from 1.79 to 1.30 with enhancing “oasis effect” was found in a paddy field (Baldocchi et al., 2016). The annual variation of α_{PT} on a wet pine forest in England ranged from 8.57 to 11.52 with a mean value of 9.5 (Shuttleworth & Calder, 1979), which is surprisingly higher than the normal values.

Table 1. Variations of the PT coefficient over wet surfaces synthesized from published papers

Type	Site Name	Range	Timescale	Reference
Open water	Ross Barnett Reservoir, USA	1.0-2.04	Sub-daily	Guo et al. (2015)
	Lake Taihu, China	1.15-1.54*	Half-Monthly	Zhang and Liu (2013)
	Lake Flevo, Netherlands	1.14-1.94	Monthly	Wang et al. (2014)
	Lake Qinghaihu, China	1.20-1.50	Monthly	De Bruin and Keijman (1979)
		1.16-1.62*	Monthly	Li et al. (2016)
	Ocean	1.17-2.18	Monthly	Yang and Roderick (2019)
Irrigated cropland	Yucheng, China	1.0-3.95**	Sub-daily	Li and Yu (2007)
Wet bare soil	Campbell, USA	1.41-3.15*	Daily	Parlange and Katul (1992)
Wetland	Tilopozo, Chile	0.60-4.80**	Sub-daily	Assouline et al. (2016),
Paddy	Twitchell, USA	1.30-1.79	Annual	Baldocchi et al. (2016)
Wet forest	Amazon	0.67-3.12	Sub-daily	Knox et al. (2016)
	Central Wales	1.16-1.79	Annual	Shuttleworth and Calder (1979)
	Norfolk, England	8.57-11.52	Annual	Shuttleworth and Calder (1979)

* The values are calculated by the data of the corresponding references.

** The values are roughly extracted from figures of the corresponding references.

In the above studies, α_{PT} showed a similar seasonal variation, which is low in warm seasons and high in cold seasons. De Bruin and Keijman (1979) found that α_{PT} over a large and shallow lake in the Netherlands reaches as high as 1.5 in April and October but as low as 1.2 in August. Similar seasonal variations in α_{PT} of 1.14 in July and 1.94 in January were reported over Lake Taihu (Wang et al., 2014). Using the half monthly data of Ross Barnett Reservoir (Zhang & Liu, 2013), the calculated α_{PT} varied between 1.15 in August and 1.54 in February. Similar variations in α_{PT} between 1.16 and 1.62 were calculated using the data of the largest high-altitude saline lake (Lake Qinghaihu) on the Qinghai–Tibet Plateau (Li et al., 2016). The seasonal variations indicated large values of α_{PT} corresponding to the small values of E_{rad} and E and vice versa. The regression line of E on E_{rad} was usually characterized with a positive intercept (De Bruin & Keijman, 1979; Parlange & Katul, 1992). Using the global ocean surface evaporation product from the Objectively Analyzed Air–Sea Flux (OAFlux) project, Yang and Roderick (2019) found a perfect linear regression relationship between the spatial variability of monthly evaporation and equilibrium evaporation over ocean surfaces, $E = 1.16E_{rad} + 10.21$ (converted from the their regression equation $E_{rad} = 0.86E - 8.78$, $R^2=0.98$). This finding implies that the

calculated α_{PT} decreases from 2.18 to 1.17 with the increase in E_{rad} from 10 W m² to 150 W m².

2.2 Wet surface SGC equation

The SGC equation over a natural evaporating surface (Han & Tian, 2018a) is expressed as

$$\frac{E}{E_{Pen}} = \frac{1}{1+m \left(\frac{x_{max} - \frac{E_{rad}}{E_{Pen}}}{\frac{E_{rad}}{E_{Pen}} - x_{min}} \right)^n}, \quad (5)$$

where x_{min} and x_{max} are the minimum and maximum values of $\frac{E_{rad}}{E_{Pen}}$, respectively. m and n can be calculated from a coefficient originated from the PT coefficient (we use α_{HT} to distinguish it from the PT coefficient) and asymmetry parameter b by making the sigmoid function approximately equal to the linear AA Equation (3).

$$\begin{cases} n = \frac{4\alpha_{HT}(1+b^{-1})(x_{0.5} - x_{min})(x_{max} - x_{0.5})}{(x_{max} - x_{min})} \\ m = \left(\frac{x_{0.5} - x_{min}}{x_{max} - x_{0.5}} \right)^n \end{cases}, \quad (6)$$

where $x_{0.5} = \frac{0.5+b^{-1}}{\alpha_{HT}(1+b^{-1})}$ is the value of $\frac{E_{rad}}{E_{Pen}}$ corresponding to $\frac{E}{E_{Pen}} = 0.5$. x_{min} and x_{max} are suggested to be 0 and 1, respectively, at the daily or monthly timescales because of the insensitivity of the SGC equation to them (Han et al., 2012; Wang et al., 2020; Zhou et al., 2020). Given Eq. (6) and using $x_{min} = 0$ and $x_{max} = 1.0$, Eq. (5) has two independent parameters α_{HT} and b . Asymmetric parameter b is found to be small in dry regions (Han et al., 2012), and increases with the land surface wetness, and approaches infinity over wet surfaces (Wang et al., 2020). This condition indicates that we can obtain an SGC equation for wet surfaces (named as wet surface SGC equation hereafter) by setting parameter b to infinity ($b^{-1}=0$) in Eq. (6). In this case, $x_{0.5} = 0.5\alpha_{HT}^{-1}$, and Eq. (6) becomes:

$$\begin{cases} n = 2 - \alpha_{HT}^{-1} \\ m = \left(\frac{1}{2\alpha_{HT}-1} \right)^n \end{cases}, \quad (7)$$

where α_{HT} is the single parameter, which controls the shape of the curve (Figure 1). If $\alpha_{HT} = 1$, the wet surface SGC equation is equal to the equilibrium evaporation $E = E_{rad}$ (lower blue line), whereas it is equal to the Penman equation $E = E_{Pen}$ (upper horizontal blue line) if $\alpha_{HT} = +\infty$. Thus, the equilibrium evaporation and Penman open water evaporation are the two limits for evaporation predicted by the wet surface

SGC equation. For the wet surface SGC equation with a specific α_{HT} , $\frac{E}{E_{Pen}}$ increases nonlinearly with $\frac{E_{rad}}{E_{Pen}}$. As shown in Figure 1, the SGC curve approaches the line of $\frac{E}{E_{Pen}} = \alpha_{HT} \frac{E_{rad}}{E_{Pen}}$ at $\frac{E}{E_{Pen}} = 0.5$ but does not exceed it. After the tangent point, the curve deviates from the line and is characterized with an obvious upper flatness part.

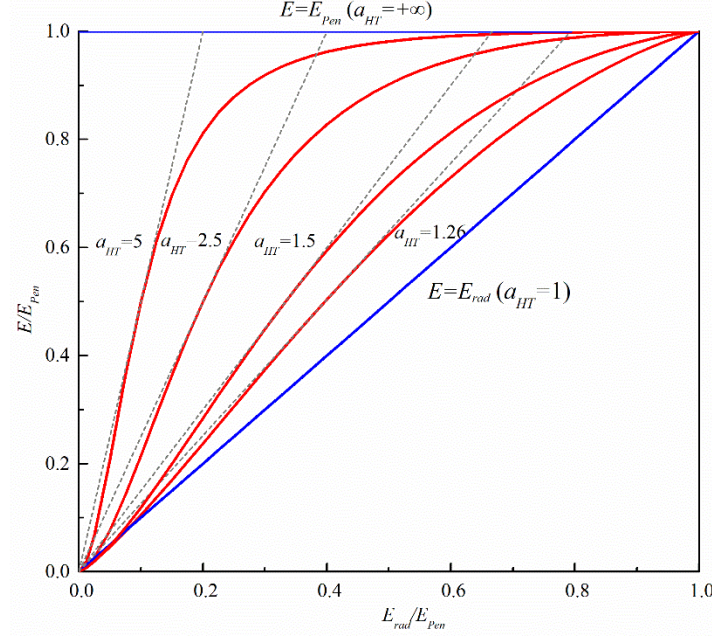


Figure 1. Plots of the wet surface SGC equation with parameters calculated by Equation (7) with varying α_{HT} values (1.26, 1.5, 2.5, and 5 are set as examples, red line). The lines of $\frac{E}{E_{Pen}} = \alpha_{HT} \frac{E_{rad}}{E_{Pen}}$ are plotted for comparison (dashed gray lines). The blue lines are the equilibrium evaporation (corresponding to $\alpha_{HT} = 1$) and Penman evaporation (corresponding to $\alpha_{HT} = +\infty$) boundary lines.

Given that $\frac{E}{E_{Pen}}$ divided by $\frac{E_{rad}}{E_{Pen}}$ is equal to E divided by E_{rad} , the PT coefficient α_{PT} in the context of Equation (2) can be derived from the wet surface SGC equation.

$$\alpha_{PT} = \frac{E}{E_{rad}} = \frac{x^{-1}}{1+m(\frac{1-x}{x})^n}, \quad (8)$$

where $x = \frac{E_{rad}}{E_{Pen}}$, and m and n are calculated from α_{HT} by using Equation (7). Thus, the wet surface SGC equation suggests a varying PT coefficient related with $\frac{E_{rad}}{E_{Pen}}$, which can be detected from the varying slope of the connecting line of the point of the sigmoid curve to the original point. Under the condition of $\frac{E}{E_{Pen}} = 0.5$, the connecting line is the tangent of the SGC curve, and the PT coefficient α_{PT} reaches its

maximum value: α_{HT} . With the increase in $\frac{E_{rad}}{E_{Pen}}$, the wet surface SGC equation suggests an increasing PT coefficient before the tangent point, but a decreasing PT coefficient after the tangent point. Taking $\alpha_{HT} = 1.5$ as an example, the calculated α_{PT} is 1.19 at $\frac{E_{rad}}{E_{Pen}} = 0.1$ and reaches its maximum value of 1.5 at $\frac{E_{rad}}{E_{Pen}} = 0.33$. With the continuous increase in $\frac{E_{rad}}{E_{Pen}}$, the calculated α_{PT} decreases to 1.26 and 1.10 when $\frac{E_{rad}}{E_{Pen}}$ increases to 0.71 and 0.89, respectively. Thus, the variation of the PT coefficient can be reflected in the wet surface SGC equation with a fixed parameter α_{HT} (denoting the maximum value of varying α_{PT}).

3 Dataset

Taihu is the third largest freshwater lake (2,400 km²) in China, with a mean depth of 1.9 m. The climate is subtropical with a mean air temperature of 16.2 °C and mean annual precipitation of more than 1,100 mm. The five eddy flux monitoring sites are inside the lake and a companion land site close to the lake (Table 2). The data were obtained from the Lake Taihu Eddy Flux Network (Lee et al., 2014). The Meiliangwan (MLW, with an average water depth of 1.8 m) site is the nearest to the shoreline (150 m), with inevitable advection effects (Wang et al., 2014). The other four sites, namely, Dapukou (DPK), Bifenggang (BFG), Xiaoleishan (XLS), and Pingtaishan (PTS), have enough open fetches and strong winds, guaranteeing that their measurements are representative of the open water. The PTS site located in the center region of the lake is the farthest from the shore. The companion land site (Dongshan (DS), above a landscape dominated by cropland and rural houses) is located at a peninsula on the southeast shore of the lake. All the six sites have an eddy covariance system, a four-component net radiometer, and a standard micrometeorological system. Water temperature probes were placed at the 20, 50, 100, and 150 cm depths for all the five lake sites. Details of the sites and instrumentation are given by Lee et al. (2014).

The wet surface SGC equation was also evaluated by using the published data of the two flux sites on Qinghaihu Lake, the largest high-altitude saline lake on the Qinghai–Tibet Plateau, China (Li et al., 2016) and Ross Barnett Reservoir, a large southern inland water in Mississippi, United States (Zhang & Liu, 2013). For Qinghaihu Lake, we used the monthly data during the ice-free period (April to October) from May 2013 to May 2015 (Table 2 in (Li et al., 2016)). For Ross Barnett

Reservoir, we used the two-year averaged half monthly means of the flux and meteorological variables in 2008 and 2009 (Table 1 in Zhang and Liu (2013)).

Table 2. Flux sites investigated in this study

Type	Site	Name	Lat.	Lon.	Periods	Reference
Lake Taihu	MLW	Meiliangwan	31.42	120.21	2010-2016 ^a	Lee et al. (2014)
	DPK	Dapukou	31.27	119.93	2011-2018 ^a	
	BFG	Bifenggang	31.17	120.40	2011-2018 ^a	
	XLS	Xiaoleishan	31.00	120.13	2012-2018 ^a	
	PTS	Pingtaishan	31.23	120.11	2013-2018 ^a	
Wetlands	WPT	Winous Point Marsh	41.46	-83.00	2011-2013 ^b	Chu et al. (2015)
	HBW	Haibei Swamp	37.62	107.32	2004-2006 ^b	Yu et al. (2006)
Paddy	MSE	Mase paddy	36.05	140.03	2002-2006 ^b	Saito et al. (2005)
	TWT	Twitchell Rice	38.11	-121.65	2009-2014 ^c	Baldocchi et al. (2016)
Croplands	DS	Dongshan	31.08	120.43	2011-2018 ^a	Lee et al. (2014)

^aThe start month of the data used is based on the study of Lee et al. (2014). ^bThe data from June to September are used. Only the days with water above the surface are used if the recorded water level data are available. ^cData from June 20 to September 20 are used to guarantee that water is above the surface

The global ocean surface evaporation product (Version 3) from the OAFflux project (Yu & Weller, 2007) was also used to evaluate the wet surface SGC equation. This product provides monthly ocean surface latent and sensible heat fluxes, near-surface air temperature, specific humidity, and wind speed at 1° spatial resolution from 1958. The ocean surface evaporation data were validated with buoy- and ship-based measurements (Yu and Weller, 2007; Yu et al., 2008). We used the monthly data of all the ocean surfaces in 2018 to evaluate the performance of the SGC equation on reproducing the spatial variability of global ocean surface evaporation. The evaluation was confined to the grid-boxes/months when the air temperature is higher than 0 °C. We did not use the grid-boxes/months with $E_{rad} < 0.1 \text{ mm day}^{-1}$ to avoid the high potential biases caused by small solar radiation or extremely low evaporation. The grid-boxes/months with E larger than 1.1 times of E_{pen} were regarded as suspicious and were excluded. A total of 375,861 grid-box/months were chosen by using this data screening procedure. We used the data of a grid-box (N25°, E120°) from 1980 to 2018 to validate the performance of the SGC equation on reproducing the temporal variability of ocean surface evaporation.

Two wetland sites and two paddy sites were investigated to further evaluate the SGC equation over the wet surfaces in addition to open water. The Winous Point

Marsh site (WPT) (N41°27', W82°59'), as a FLUXNET site, is located in the Winous Point Marsh Conservancy along the shore of Lake Erie in northwestern Ohio, United States (Chu et al., 2014). The marsh was managed to maintain year-round inundation with the lowest water levels in September. Within the 0–250 m fetch of the tower, the marsh comprises 42.9% of floating-leaved vegetation and 52.7% of emergent vegetation from late May to early October, and the height of the canopy nearby the flux tower is 0.4–0.6 m (Chu et al., 2015).

The Haibei alpine swamp site (HBW) with elevation of 3,160 m (N41.46, E107.32), as a ChinaFLUX site, is located at the Haibei Alpine Meadow Ecosystem Research Station in the northeast of the Qinghai–Tibet Plateau (Li et al., 2007). The alpine marsh vegetation is distributed in surface depressions with an average canopy height of 0.5 m, and most of the area are covered by water during June to September.

The Mase paddy site (JP-MSE) (N36°03', E140°01'), as an AsiaFlux site, is located at a rural area of Tsukuba City in Central Japan (Saito et al., 2005). Around the site, irrigated rice fields extend to an area of 1.5 km from north to south by 1 km from east to west. The paddy fields around the tower were managed as single rice-cropping fields and were flooded from late April to the August during the study period.

The Twitchell rice paddy site (TWT), also a FLUXNET site is located at Twitchell Island in the Sacramento-San Joaquin Delta, California, USA. The field was flooded throughout the growing season and harvested between late September and late October. The measurements were conducted from April, 2009, with the flooded rice field less than 1 km² in area during the first year. The area of flooded rice and wetlands expanded to approximately 6 km² by 2014 (Knox et al., 2016), resulting in a reducing “oasis effect” (Baldocchi et al., 2016).

Following Wang et al. (2014), the components of the energy balance residual, except for water heat storage, are ignored at the Taihu lake sites. The water heat storage is calculated with the time rate of change in the depth-weighted mean water temperature. At Qinghaihu Lake and Ross Barnett Reservoir, the energy balance residual is supposed to be $Res = R_n - LE - H$, following the studies of Li et al. (2016) and Zhang and Liu (2013). For the ocean grid, $Res = R_n - LE - H$.

At the two wetland sites, the data on the components of energy balance residual Res are unavailable. However, at WPT, the slope of the regression line of daily $LE +$

H on net radiation $R_n - Res$ is 0.70 according to the energy balance closure analysis of Chu et al. (2015). We calculated that the regression line of daily $LE + H$ on R_n is 0.59 ($R^2 = 0.68$) and deduced that Res is approximately 15% of R_n . We also used this proportion at HBW.

At the two paddy sites, the soil heat flux data are available, whereas the other components of Res are unavailable. Baldocchi et al. (2016) obtained a daily energy balance of $LE + H + Res = 0.835R_n + 0.782$ ($R^2 = 0.90$) at TWT. We calculated an energy balance of $LE + H + G = 0.847R_n + 0.782$, ($R^2 = 0.91$). This finding implies that the components besides the soil heat flux only occupy approximately 1.2% of R_n . Thus, we ignored them for the two paddy field sites.

At the lake sites and ocean grid with flat surfaces, we used the wind function (given in $\text{mm day}^{-1} \text{ kPa}^{-1}$) following Penman (1948)

$$f(u_2) = 2.6(1 + 0.54u_2), \quad (9)$$

where u_2 is the wind speed 2 m above the ground surface, which is converted from the wind speed (u_z) by assuming a power dependency on the measurement height z ,

$u_2 = u_z \left(\frac{2}{z}\right)^{\frac{1}{7}}$ (Brutsaert, 2005). At the wetland and paddy field sites, we used the

wind function derived on the basis of Monin–Obukhov similarity theory assuming neutral conditions

$$f(u_z) = \frac{0.622\kappa^2 u_z}{R_d T_a \ln\left[\left(\frac{z-d_0}{z_{0m}}\right)\right] \ln\left[\left(\frac{z-d_0}{z_{0v}}\right)\right]}, \quad (10)$$

where κ is the von Karman constant, R_d is the specific gas constant for dry air, and T_a is the mean air temperature. z_{0m} is the roughness lengths for momentum, which depends on the vegetation covering the surface. We used the value of 0.12 times of the maximum canopy height, following Allen et al. (1998). At WPT and HBW, z_{0m} was estimated to be 0.06 in accordance with their canopy height around 0.5 m. At MSE and TWT, the maximum canopy height is approximately 1.2 m, and z_{0m} during the growing season is determined to be 0.15 m. The zero-plane displacement height d_0 and the roughness lengths for water vapor z_{0v} are approximated as $d_0 = 5.5z_0$ and $z_{0v} = 0.1z_{0m}$.

All the variables of the flux sites were recorded every 30 min and were initially processed into daily means. The monthly data processed from the daily data were used for the sites of Lake Taihu. We adopted the following methods to screen the data. The data throughout the year during the study period (Table 2) were used over the

lake sites and the ocean grid. Only the data from June to September were used for the wetland and paddy sites to guarantee ample water availability and relatively stable canopy heights. If the recorded water level data are available, only the days with water above the surface were used.

The Bowen ratio closure, which corrects the latent heat fluxes (Twine et al., 2000), was applied on a daily (Brutsaert et al., 2017; Zhang et al., 2017) or monthly basis (Wang et al., 2014). The method is formulated as

$$E = \frac{R_n - Res}{LE_u + H} \times E_u, \quad (11)$$

where H is the sensible heat flux, and E_u is the unadjusted actual evaporation.

The data excluded from the study comprise the days that recorded missing data for extended time periods, with negative values of $(R_n - Res)$ or E . The data with E larger than 1.1 times of E_{pen} or less than E_{rad} are regarded as suspicious and are excluded.

m and n of the wet surface SGC equation are determined by using Equation (7). Thus, only one parameter is calibrated for the SGC (α_{HT}) and PT (α_{PT}^c) equations by minimizing the root mean square error (RMSE) of the actual evaporation. The mean absolute error (MAE) and Nash–Sutcliffe coefficient of efficiency (NSE) are used to evaluate the model performance on evaporation estimation.

4 Results from open water surfaces

4.1 Nonlinear dependence of E on E_{rad} and bias of the linear PT equation at Lake Taihu sites

The daily E from June 2013 to December 2018 at PTS shows a significant dependence on E_{rad} ($E = 1.25E_{rad}$, $R^2=0.99$, Figure 2(a)). The very high correlation indicates that the linear PT equation with an optimized coefficient of 1.25 can simulate E well. However, the linear PT equation underestimates the evaporation for most of the days with small values of E_{rad} (656 of the 807 days with $E_{rad} < 2 \text{ mm day}^{-1}$ for instance). The mean value of the estimated E of these days with $E_{rad} < 2 \text{ mm day}^{-1}$ is $1.29 \pm 0.70 \text{ mm day}^{-1}$, which is approximately 14% lower than that of the observed E ($1.49 \pm 0.78 \text{ mm day}^{-1}$) (Table 3). On the contrary, the linear PT equation overestimates the evaporation for most of the days with large values of E_{rad} (60 of the 82 days with $E_{rad} > 6.5 \text{ mm day}^{-1}$ for instance). The mean value of the estimated E of these days is $9.70 \pm 1.45 \text{ mm day}^{-1}$, which is approximately 3% higher than that of the observed E ($9.42 \pm 1.36 \text{ mm day}^{-1}$). However, the underestimation and overestimation are offset if

averaging over the period, and the mean values of the estimated ($3.34 \pm 2.43 \text{ mm day}^{-1}$) and observed E ($3.43 \pm 2.34 \text{ mm day}^{-1}$) show trivial difference.

The other four lake sites exhibit similar patterns (Table 3) with optimized α_{PT}^c close to 1.26 (Table 4). The underestimation of the linear PT equation on the mean value of E for the days with $E_{rad} < 2 \text{ mm day}^{-1}$ is approximately 10%–16%, whereas the overestimation for the days with $E_{rad} > 6.5 \text{ mm day}^{-1}$ is approximately 3%–5%.

Table 3. Mean values of the observed and estimated E by the linear PT and SGC equations for the data group with small and large E_{rad} (mm day^{-1})

		Group with small E_{rad}^*			Group with large E_{rad}^{**}		
	Sites	Observed	PT estimated	SGC estimated	Observed	PT estimated	SGC estimated
Daily	MLW	1.43±0.79	1.20±0.71	1.35±0.77	8.94±1.15	9.38±1.21	9.18±1.10
	DPK	1.40±0.79	1.22±0.71	1.35±0.77	9.47±1.37	9.72±1.40	9.57±1.29
	BFG	1.48±0.78	1.28±0.70	1.42±0.75	8.76±0.80	9.15±0.82	8.90±0.77
	XLS	1.35±0.77	1.21±0.71	1.34±0.76	9.12±1.04	9.43±1.02	9.12±1.09
	PTS	1.49±0.78	1.29±0.70	1.44±0.75	9.42±1.36	9.70±1.45	9.53±1.35
Monthly	MLW	1.50±0.60	1.22±0.57	1.36±0.61	5.87±0.19	6.17±0.18	6.10±0.25
	DPK	1.50±0.54	1.30±0.55	1.41±0.56	6.05±0.63	6.25±0.59	6.16±0.56
	BFG	1.35±0.45	1.18±0.45	1.31±0.48	6.22±0.47	6.43±0.47	6.22±0.50
	XLS	1.29±0.48	1.16±0.50	1.29±0.50	6.19±0.54	6.36±0.47	6.12±0.54
	PTS	1.48±0.45	1.34±0.48	1.46±0.50	6.40±0.53	6.57±0.57	6.44±0.53

* $E_{rad} < 2 \text{ mm day}^{-1}$ at the daily and monthly timescales

** $E_{rad} > 6.5 \text{ mm day}^{-1}$ at the daily timescale and $E_{rad} > 4.5 \text{ mm day}^{-1}$ at the monthly timescale

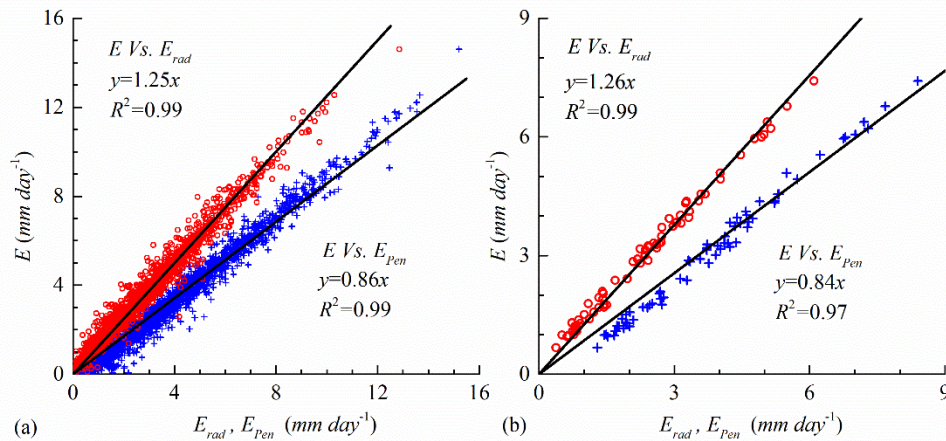


Figure 2. Plots of E with respect to E_{rad} and E_{pen} at PTS at the (a) daily and (b) monthly time scales

The plot of monthly E versus E_{rad} from June 2013 to December 2018 at PTS exhibits similar features (Figure 2(b)). The linear PT equation with optimized $\alpha_{HT}=1.26$ underestimates E for 23 of the 28 months with $E_{rad} < 2 \text{ mm day}^{-1}$ (Table 3) (the mean values of the observed and estimated E are 1.48 ± 0.45 and $1.34 \pm 0.48 \text{ mm}$

day⁻¹, respectively. However, it overestimates E for 6 of 7 months with $E_{rad} > 4.5$ mm day⁻¹ (the mean values of the observed and estimated E are 6.40 ± 0.53 and 6.57 ± 0.57 mm day⁻¹, respectively). The magnitudes of the underestimation and overestimation on the mean values of E are slightly lower than those at the daily timescale.

The daily time series of observed E and the radiation (E_{rad}) and aerodynamic (E_{aero}) components of E_{Pen} during 2014 (322 days left after excluding the suspicious data) at the central lake site of PTS are shown in Figure 3 (a) as an example. The daily E_{rad} at PTS varies significantly between 0.01 and 9.01 mm, with a mean value of 2.41 ± 1.63 mm day⁻¹. The daily E_{aero} at PTS varies between 0.03 and 4.07 mm day⁻¹ (a mean value of 1.36 ± 0.66 mm day⁻¹), and is much smaller than E_{rad} during summer. Ranging between 0.02 and 11.32 mm day⁻¹ (with a mean value of 3.12 ± 1.95 mm day⁻¹), the daily E at PTS shows many similar pulses with E_{rad} during the warm seasons, but several similar pulses with E_{aero} during the cold seasons.

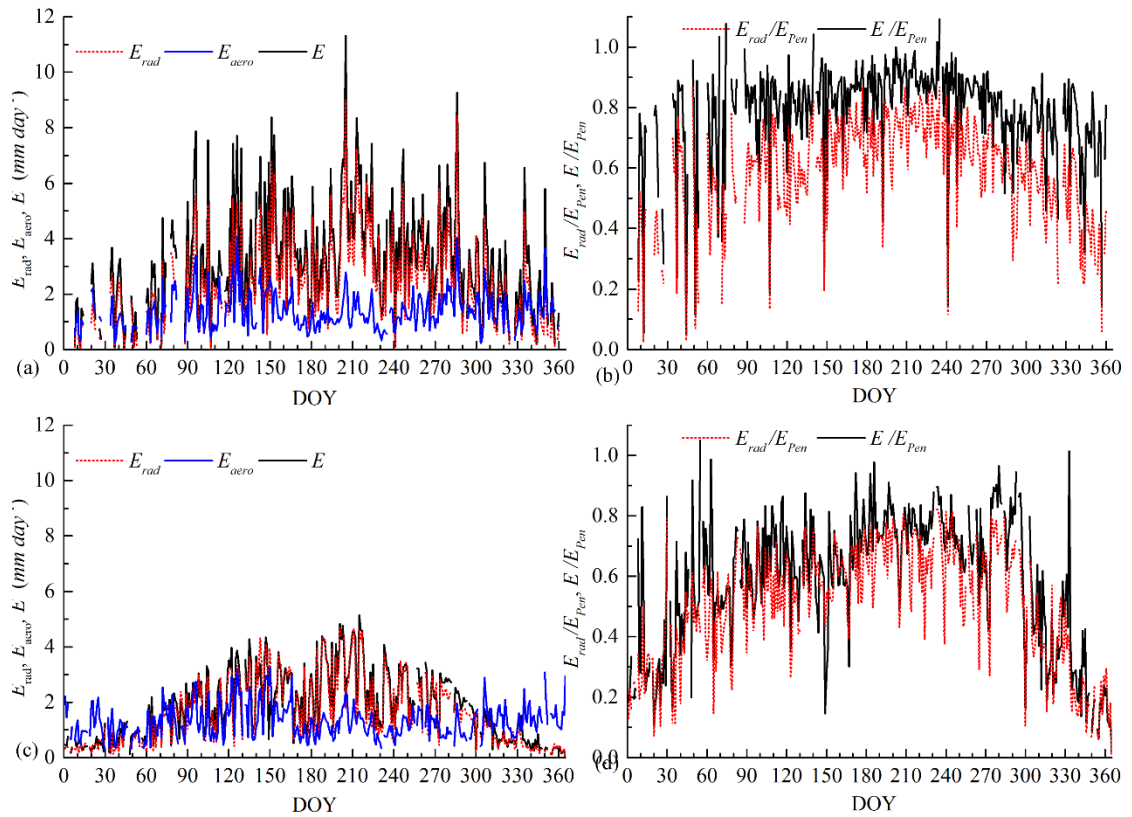


Figure 3. Daily time series of observed E , the radiation (E_{rad}) and aerodynamic (E_{aero}) terms of E_{Pen} , and $\frac{E}{E_{Pen}}$ and $\frac{E_{rad}}{E_{Pen}}$ during 2014 at the lake site PTS (a, b) and the cropland site DS (c, d).

The daily E from June 2013 to December 2018 at PTS is significantly correlated with E_{Pen} ($E_{rad} + E_{aero}$), $E = 0.86E_{Pen}$, $R^2=0.99$. However, the regression equation

overestimates E under the conditions of small values of E but underestimates E under the conditions of large values of E (Figure 2(a)), which is opposite to that of the linear PT equation. The results indicate that the wet surface evaporation at PTS is also affected by varying E_{aero} , which can be detected from their correlation ($E = 0.23E_{aero} + 0.67$, $R^2=0.56$). Besides, the correlation between E_{rad} and E_{aero} is weak ($E_{aero} = 0.25E_{rad} + 0.80$, $R^2=0.46$). The plots of monthly E versus E_{rad} and E_{Pen} exhibit similar nonlinear characteristics to those at the daily time scale (Figure 2(b)).

Above results indicate that the variations of E_{aero} cannot be fully explained by a constant proportion of E_{rad} . E_{aero} should be considered subtly rather than a constant proportion of E_{rad} for a better estimation of the wet surface evaporation.

4.2 Nonlinear dependence of E/E_{Pen} on E_{rad}/E_{Pen} and performance of the SGC equation at Lake Taihu sites

As shown in Figure 3(b), daily $\frac{E_{rad}}{E_{Pen}}$ during 2014 at PTS exhibits an obvious variation between 0.03 and 0.87 (with a mean value of 0.59 ± 0.17), and $\frac{E}{E_{Pen}}$ varies from 0.05 to 1.09 with a mean value of 0.78 ± 0.18 . Daily $\frac{E}{E_{Pen}}$ and $\frac{E_{rad}}{E_{Pen}}$ exhibit similar seasonal variations of low values in winter but high values in summer. The simultaneous variations of $\frac{E}{E_{Pen}}$ and $\frac{E_{rad}}{E_{Pen}}$ are similar to those at the land site DS (Figures 3 (d)). As shown in the scatter plots of daily $\frac{E}{E_{Pen}}$ versus $\frac{E_{rad}}{E_{Pen}}$ (Figure 4), $\frac{E}{E_{Pen}}$ appears to be related to $\frac{E_{rad}}{E_{Pen}}$ at all the five lake sites, which is similar to that at the land site DS. However, the scatter points of the lake sites are located higher than those of the land site in the state space of $(\frac{E}{E_{Pen}}, \frac{E_{rad}}{E_{Pen}})$.

At the five lake sites, $\frac{E}{E_{Pen}}$ increases nonlinearly with $\frac{E_{rad}}{E_{Pen}}$, and the growth rate decreases when $\frac{E_{rad}}{E_{Pen}}$ is larger than 0.5, showing an obvious flatness part. The wet surface SGC equation with optimized α_{HT} fits the scatter points well for all the five lake sites (Table 4, Figure 4). The scatter plots and the values of the optimized α_{HT} of the five lake sites differ slightly, which is consistent with the findings of Wang et al. (2014) that the energy fluxes showed minimal spatial variations across the lake. However, the biases of the linear PT equation in the state space of (E, E_{rad}) shown in Figure 3 are amplified, where the PT line obviously deviates from the scatter plots.

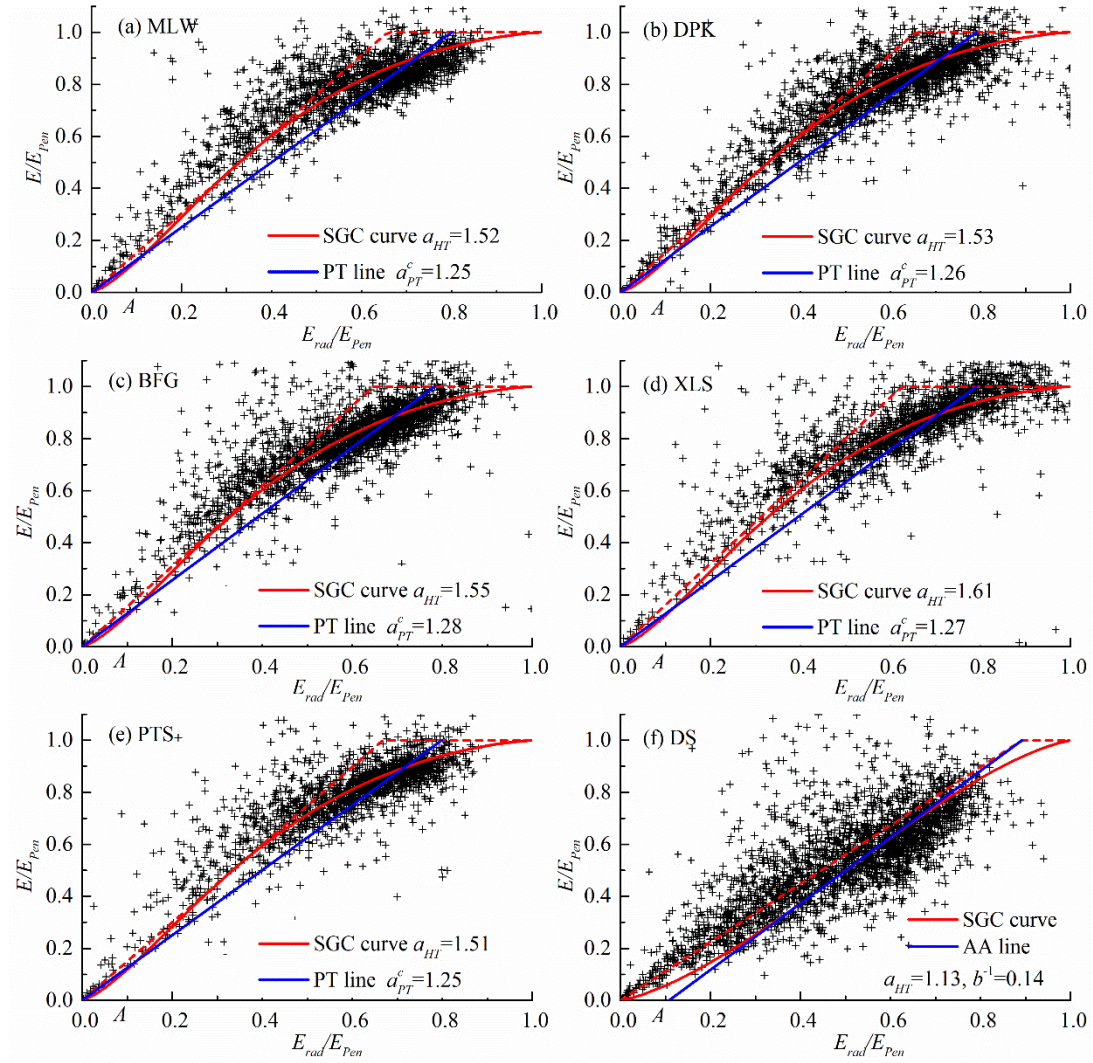


Figure 4. Plots of daily $\frac{E}{E_{pen}}$ with respect to $\frac{E_{rad}}{E_{pen}}$ at the five lake sites (a-e) on Lake Taihu compared with the optimized wet surface SGC equation and the linear PT equation. The land site (f) is also compared with the original SGC and AA equations.

Table 4. Optimized parameters and performance of the wet surface SGC equation and linear PT equation in estimating daily wet surface evaporation (mm day^{-1})

Type	Site	Wet surface SGC equation				Linear PT equation			
		α_{HT}	MAE mm day^{-1}	RMSE mm day^{-1}	NSE	α_{PT}^c	MAE mm day^{-1}	RMSE mm day^{-1}	NSE
Lake (Taihu)	MLW	1.52	0.23	0.30	0.98	1.25	0.33	0.44	0.96
	DPK	1.53	0.22	0.31	0.98	1.26	0.32	0.45	0.96
	BFG	1.55	0.21	0.29	0.98	1.28	0.31	0.42	0.96
	XLS	1.61	0.19	0.28	0.98	1.27	0.28	0.39	0.97
	PTS	1.51	0.20	0.29	0.98	1.25	0.30	0.41	0.97
Wetland	WPT	1.31	0.18	0.23	0.97	1.24	0.20	0.26	0.97
	HBW	1.29	0.34	0.46	0.94	1.24	0.34	0.45	0.94
Paddy	MSE	1.69	0.32	0.42	0.95	1.41	0.33	0.49	0.93
	Twt	1.73	0.64	0.83	0.69	1.70	0.67	0.85	0.68

At the monthly time scale, the growth of $\frac{E}{E_{Pen}}$ on $\frac{E}{E_{Pen}}$ exhibits the same nonlinear characteristic at all the five lake sites, and the optimized PT lines deviate from the scatter points (Figure 5). By contrast, the wet surface SGC equation with optimized α_{HT} fits the scatter points better (Table 5). The optimized α_{HT} at the monthly time scale is slightly smaller than that at the daily time scale because the SGC equation perform as a convex function for most of the points.

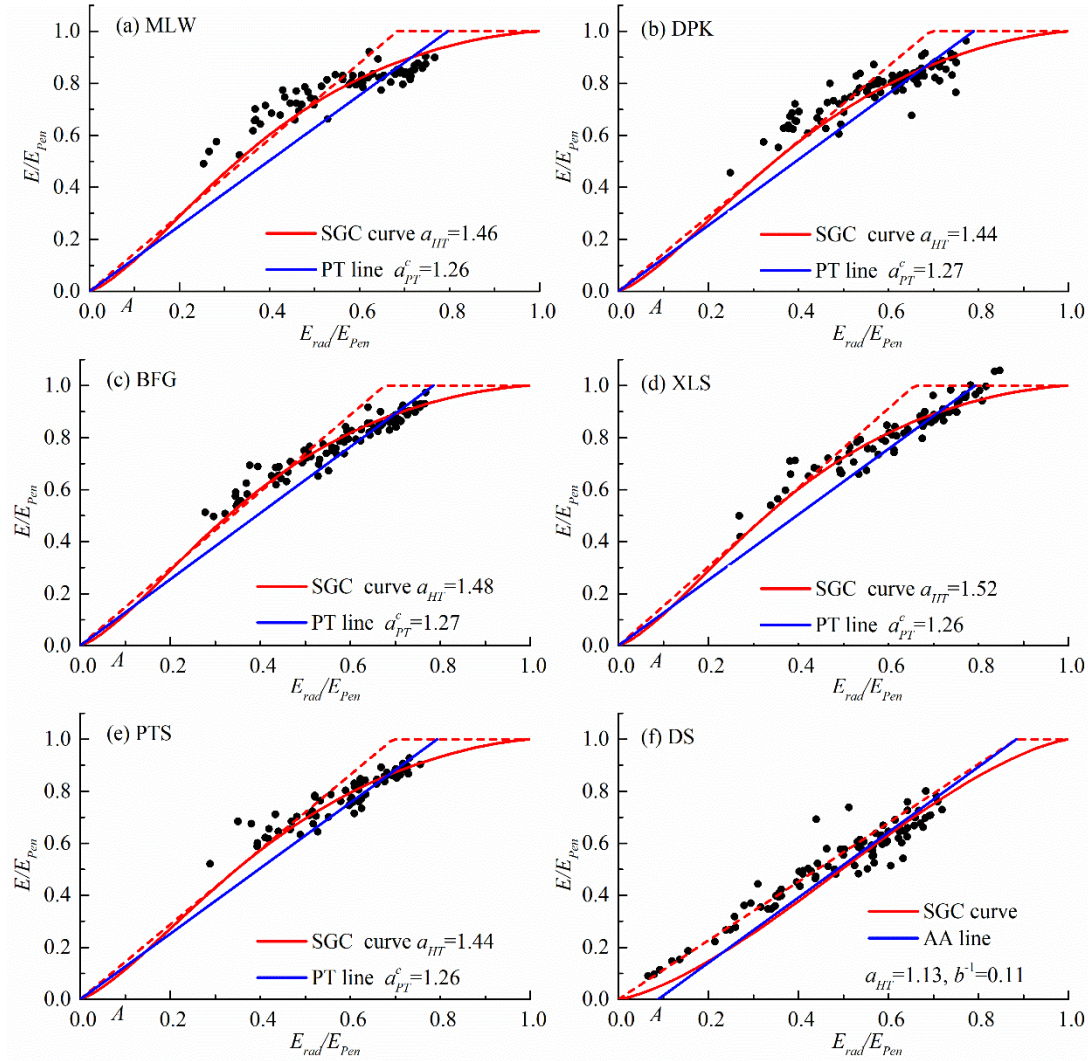


Figure 5. Plots of monthly $\frac{E}{E_{Pen}}$ with respect to $\frac{E}{E_{Pen}}$ at the five lake sites (a-e) on Lake Taihu compared with the optimized wet surface SGC equation and linear PT equation. The land site (f) is also compared with the original SGC and AA equations.

Table 5. Optimized parameters and performance of the wet surface SGC equation and linear PT equation in estimating monthly wet surface evaporation

Lake and site		Wet surface SGC equation				Linear PT equation			
		α_{HT}	MAE mm day^{-1}	RMSE mm day^{-1}	NSE	α_{PT}^c	MAE mm day^{-1}	RMSE mm day^{-1}	NSE
Lake (Taihu)	MLW	1.46	0.15	0.18	0.98	1.26	0.25	0.28	0.96
	DPK	1.44	0.12	0.15	0.99	1.27	0.20	0.24	0.98
	BFG	1.48	0.08	0.10	1.00	1.27	0.16	0.19	0.99
	XLS	1.52	0.10	0.13	0.99	1.26	0.14	0.17	0.99
	PTS	1.44	0.09	0.11	1.00	1.26	0.15	0.18	0.99
Ross Barnett Reservoir		1.31	0.09	0.10	0.99	1.22	0.13	0.16	0.98
Qinghaihu Lake		1.44	0.15	0.19	0.89	1.29	0.19	0.25	0.81
Ocean	Spatial	1.49	0.14	0.18	0.99	1.28	0.23	0.28	0.97
	Temporal	1.45	0.04	0.05	1.00	1.24	0.12	0.15	0.99

The biases of the linear PT equation were amended by the wet surface SGC equation (Table 3). Taking an example of PTS (Figure 6), the mean value of the estimated E by the wet surface SGC equation for the days with $E_{rad} < 2 \text{ mm day}^{-1}$ ($1.44 \pm 0.75 \text{ mm day}^{-1}$) is 4% lower than that of the observed E , which is an obvious improvement than 14% by the linear PT equation. By contrast, the mean value of the estimated E by the wet surface SGC equation for the days with $E_{rad} > 6.5 \text{ mm day}^{-1}$ ($9.53 \pm 1.35 \text{ mm day}^{-1}$) is 1% higher than the observed E , which is also an improvement than 3% by the linear PT equation. The improvements of the wet surface SGC equation on the linear PT equation can be found at all the five lake sites at the daily and monthly timescales (Table 3).

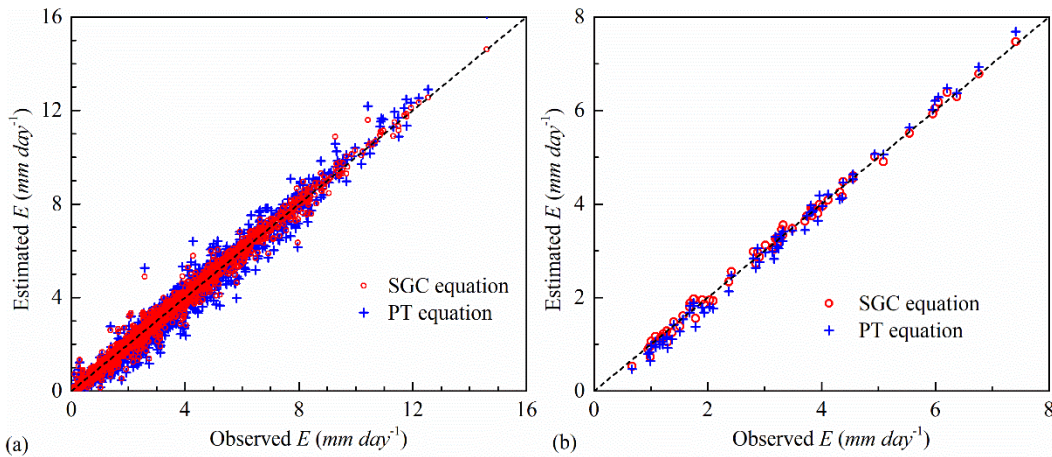


Figure 6. Plots of the estimated evaporation by the wet surface SGC equation and the linear PT equation on the observed evaporation at PTS, Lake Taihu.

For all the days or months, the wet surface SGC equation outperforms the linear PT equation on estimating evaporation at all the five lake sites at the daily and monthly timescales (Tables 4 and 5). Taking PTS site as an example, the mean value of RMSE

of the SGC equation decreases from 0.41 mm day^{-1} to 0.29 mm day^{-1} at the daily timescale compared with the linear PT equation. The MAE decreases from 0.30 mm day^{-1} to 0.20 mm day^{-1} , and the NSE increases from 0.97 to 0.98. At the monthly timescale, the improvement is still visible.

4.3 Two other lakes

The wet surface SGC equation with optimized α_{HT} (1.44 and 1.31) fitted the relationships between (semi-) monthly E/E_{Pen} and E_{rad}/E_{Pen} well at the sites of Qinghaihu Lake and Ross Barnett Reservoir (Figure 7). Its performance on evaporation estimation improved (Table 4) by amending the bias of the linear PT equation.

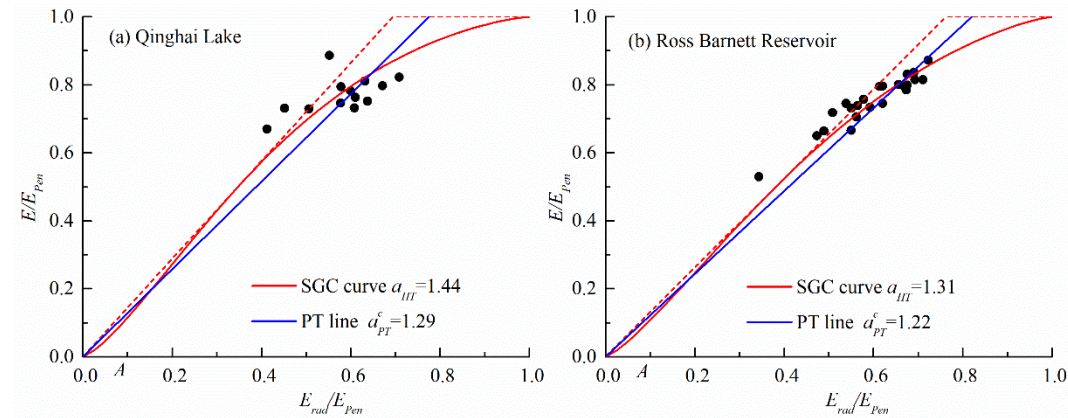


Figure 7. Plots of $\frac{E}{E_{Pen}}$ with respect to $\frac{E_{rad}}{E_{Pen}}$ at the flux sites on (a) Lake Qinghaihu and (b) Ross Barnett Reservoir, compared with the wet surface SGC equation and linear PT equation.

4.4 Ocean surfaces

Similar to the lake sites, the linear PT equation with optimized $\alpha_{PT}^c=1.28$ performs well over the grid-boxes/months of the ocean surfaces in 2018 (Figure 8(a)). It underestimates the evaporation for small values of E_{rad} but overestimates for large values of E_{rad} . This condition can be detected from the positive intercept of the regression line of E versus E_{rad} , $E = 1.14E_{rad} + 0.46$, $R^2=0.987$ (mm day^{-1}). The results are consistent with Yang and Roderick (2019)'s work on the spatial variability of evaporation on the global ocean. Similar to the results of lake sites, E of the ocean grid is highly correlated with E_{Pen} , $E = 0.84E_{Pen}$, $R^2=0.989$ (Figure 8(a)). Compared with the linear PT equation, the wet surface SGC equation with optimized $\alpha_{HT}=1.49$ fitted the relationships between monthly $\frac{E}{E_{Pen}}$ and $\frac{E_{rad}}{E_{Pen}}$ better (Figure 8(b)) and improved the performance on evaporation estimation (Table 5).

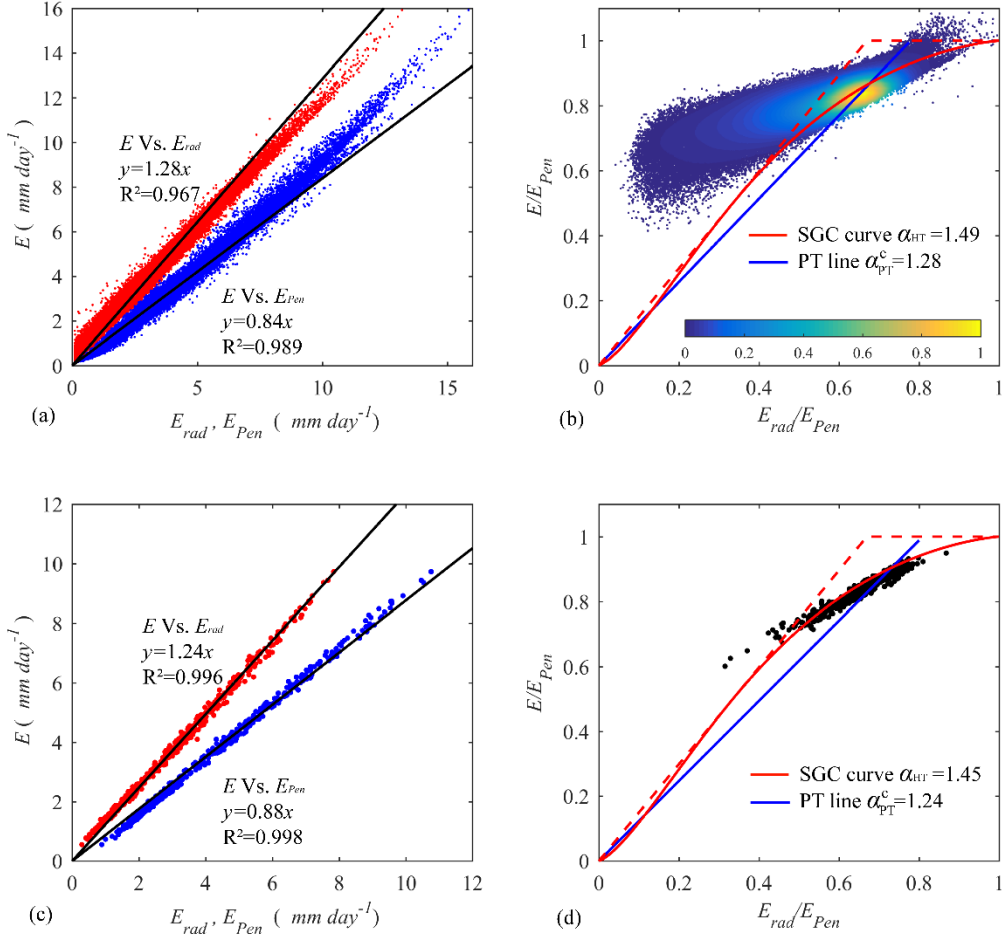


Figure 8. Plots of E with respect to E_{rad} and E_{Pen} and their regression lines and $\frac{E}{E_{Pen}}$ with respect to $\frac{E_{rad}}{E_{Pen}}$ on (a, b) the global ocean surface in 2018 (color bar represents data density), and (c, d) a selected grid-box from 1980 to 2018 compared with the wet surface SGC equation and the linear PT equation.

For the selected ocean grid-box, the wet surface SGC equation reproduces the temporal variability of monthly ocean surface evaporation from 1980 to 2018 well and amends the bias of the linear PT equation (Figures 8 (c, d)). The results are consistent with those for the spatial distribuion.

5 Evaluation on wetlands and paddy fields

At the two wetland sites and two paddy field sites, the wet surface SGC equation fits the relationship between daily E/E_{Pen} and E_{rad}/E_{Pen} well. The optimized α_{HT} at the two wetland sites (1.31 and 1.29 for WPT and HBW, respectively) are lower than those at the lake site, whereas the optimized α_{HT} at the paddy sites (1.69 and 1.73 for MSE and TWT, respectively) are larger. However, the nonlinear characteristics of the growth of E/E_{Pen} on E_{rad}/E_{Pen} are unremarkable compared with the open water

surfaces. The improvements of the wet surface SGC equation compared with the linear PT equation are unremarkable. Taking the RMSE as an index, it improves from 0.26, 0.49, and 0.85 mm day⁻¹ to 0.23, 0.42, and 0.83 mm day⁻¹ at WPT, MSE, and TWT, respectively. At HBW, the performance of the wet surface SGC equation and PT equation slightly differs (the RMSEs are 0.40 and 0.41 mm day⁻¹, respectively).

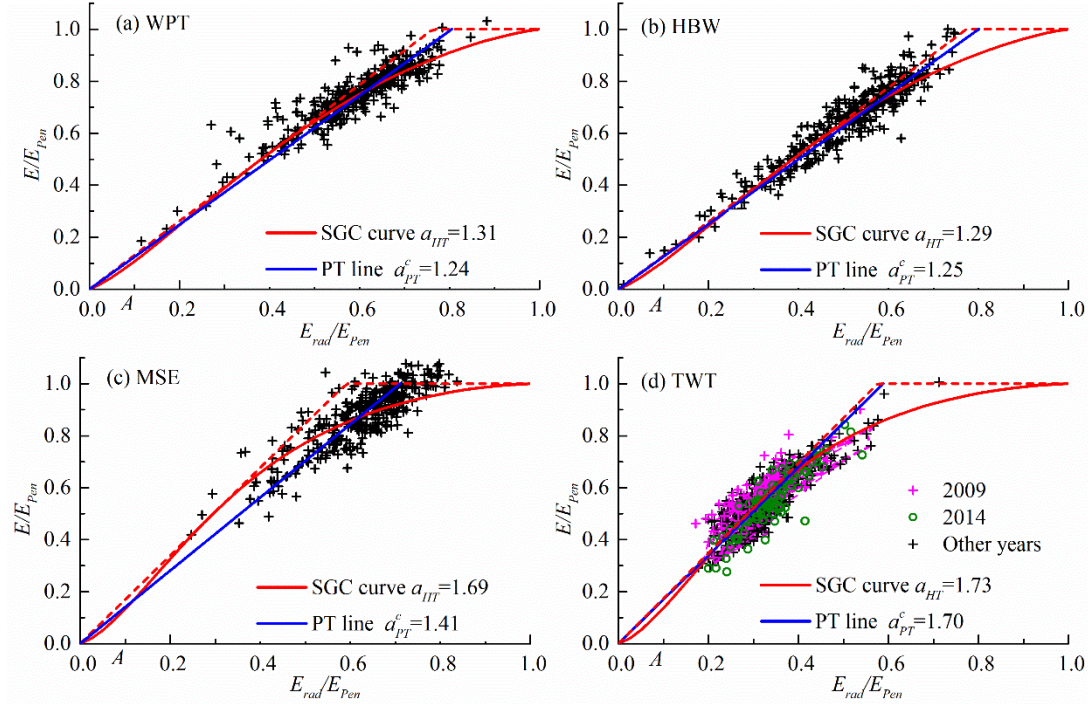


Figure 9. Plots of daily $\frac{E}{E_{pen}}$ with respect to $\frac{E_{rad}}{E_{pen}}$ at two wetlands sites: (a) WPT and (b) HBW, and two paddy sites: (c) MSE and (d) TWT compared with the wet surface SGC equation and PT equation.

6 Discussions

6.1 Capturing varying PT coefficient

The linear PT equation with optimized α_{PT}^c performs well for all the wet surfaces in this study, and the optimized α_{PT}^c are equal or extremely close to the widely accepted value of 1.26, except for the two paddy field sites (Table 4 and 5). However, the opposite biases under conditions with small and large values of $\frac{E_{rad}}{E_{pen}}$ (also E_{rad}) imply that the fixed α_{PT}^c is a result of the compromise between the two above conditions. The departures of the scatter points from the PT line in the state space $[\frac{E_{rad}}{E_{pen}}, \frac{E}{E_{pen}}]$ imply a varying coefficient α_{PT} over the wet surface. Taking the PTS site as an example (Figure 10(a)), α_{PT} shows a large variation versus $\frac{E_{rad}}{E_{pen}}$. The theoretical curve derived from the wet surface SGC equation can effectively present

the decrease in α_{PT} with $\frac{E_{rad}}{E_{Pen}}$ larger than 0.5. However, it is an improvement of the linear PT equation with a fixed coefficient. This condition explains why the wet surface SGC equation performs better than than linear PT equation on the open water surfaces, as shown in Section 4.

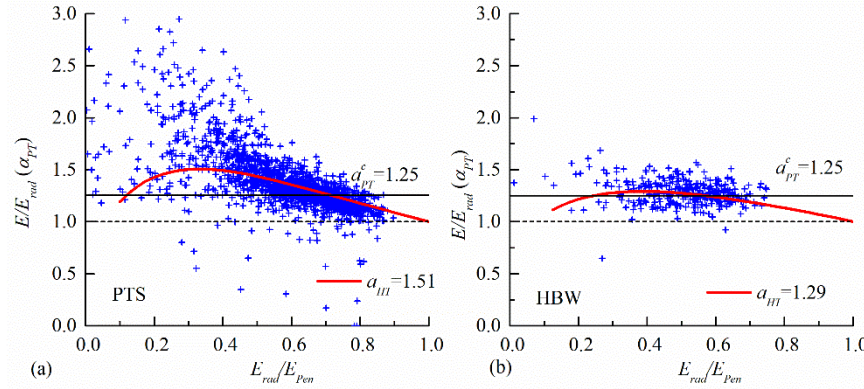


Figure 10. Plots of daily $\frac{E}{E_{rad}}$ (the varying PT coefficient α_{PT}) with respect to $\frac{E_{rad}}{E_{Pen}}$ at (a) the lake site PTS and (b) the wetland site HBW, compared with the calibrated fixed α_{PT}^c of the linear PT equation (solid line) and the theoretical curve derived from the wet surface SGC equation (red curve).

However, α_{PT} varies slightly at the wetland site HBW. The theoretical curve of α_{PT} on $\frac{E_{rad}}{E_{Pen}}$ derived from the SGC equation is flat and differs slightly with the optimized $\alpha_{PT}^c=1.25$ line for the days with $\frac{E_{rad}}{E_{Pen}}$ between 0.2 and 0.7 (Figure 10(b)). The weak variations of the PT coefficient are the reason why the improvement of the wet surface SGC equation on the linear PT equation is unremarkable at the wetland and paddy sites. At these four sites, the study was conducted during June to September, and the cold reasons were not involved to avoid that the land surfaces were not saturated. Then, the variations of the PT coefficient may be limited. However, the effects of vegetation on the different variations of the PT coefficient at the wetland and paddy sites to the open water surfaces need further studies.

6.2 Effects of advection on α_{HT}

As shown in the above plots of $\frac{E}{E_{Pen}}$ with respect to $\frac{E_{rad}}{E_{Pen}}$, a fair amount of scatter points is located outside the SGC curves with a fixed α_{HT} , especially under the conditions with small $\frac{E_{rad}}{E_{Pen}}$. As shown in Figure 10(a), the theoretical curve of α_{PT} from the wet surface SGC equation is below the scatter points with $\frac{E_{rad}}{E_{Pen}}$ smaller than

0.4 at PTS. The above biases cannot be explained by random errors and indicate that the wet surface SGC equation with a fixed α_{HT} only partially captures the variations of α_{PT} . Thus, a varying α_{HT} is required for a better estimation of evaporation by the wet surface SGC equation. However, a question may arise what factors control α_{HT} ?

Advection of hot and dry air is a main factor of the varying α_{PT} , which enlarges the wet surface evaporation rate. Considering that the wet surface SGC equation with a fixed α_{HT} only partially captures the varying α_{PT} (Figure 10), α_{HT} would be affected by the advection. At TWT, Baldocchi et al. (2016) pointed out that the advection effects declined along with the expansion of the flooded land area from less than 1 km² to more than 5 km² during the six study years. At the same time, the optimized α_{HT} at TWT declined from 1.90 in 2009 to 1.65 in 2014 (Table 5). As shown in Figure 9(d), the scatter points in 2014 are below their counterparts in 2009.

Table 5. Optimized parameters and performance of the wet surface SGC equation and the linear PT equation in estimating evaporation (mm day⁻¹) at the paddy site TWT from 2009 to 2014 with decreasing “oasis effect”

Year	SGC				PT equation			
	α_{HT}	MAE	RMSE	NSE	α_{PT}^c	MAE	RMSE	NSE
2009	1.90	0.68	0.89	0.72	1.85	0.74	0.94	0.69
2010	1.70	0.52	0.68	0.64	1.67	0.54	0.70	0.62
2011	1.77	0.59	0.75	0.62	1.71	0.65	0.81	0.56
2012	1.61	0.69	0.87	0.35	1.60	0.69	0.86	0.37
2013	1.77	0.55	0.70	0.83	1.74	0.59	0.73	0.81
2014	1.65	0.45	0.57	0.87	1.62	0.44	0.57	0.87

Advections may play a role in determining the different values of α_{HT} among the three types of wet surfaces. For the two wetland sites, their differences with the surroundings are unremarkable than the lake and paddy sites. The weak advection effect is a possible reason why the values of α_{HT} are lower than the other sites. The two paddy sites are located in small patches around 1 km², which are significantly affected by the enhanced advections. Thus, the optimized α_{HT} at the two paddy field sites are larger than those at other the sites.

Under the conditions with small values of $\frac{E_{rad}}{E_{Pen}}$ that probably occur with small radiation energy inputs, the advection effects are significant (Morton, 1983), and the evaporation rate is underestimated by the wet surface SGC equation with a specific α_{HT} . This condition may be one of the reasons why many observed scatter points of $\frac{E}{E_{Pen}}$ with respect to $\frac{E_{rad}}{E_{Pen}}$ are located above the SGC curves with small values of $\frac{E_{rad}}{E_{Pen}}$,

and many points are above the theoretical curve with fixed α_{HT} in Figure 10 (a). Thus, α_{HT} would be large under the conditions with small values of $\frac{E_{rad}}{E_{Pen}}$, thereby suggesting further studies on the seasonal variations of α_{HT} over open water surfaces.

6.3 Implication for further extension of the complementary principle

The complementary principle was originally proposed for the evaporation taking place from “a sufficiently large and homogeneous surface” (Brutsaert, 2015), where the advection effects of heat and water vapor from the outside are negligible or changeless (Brutsaert & Stricker, 1979; Han & Tian, 2018b; Morton, 1983). The complementary principle assumes that the land surface wetness can be effectively detected from the drying power of air with a constant radiation energy input (Brutsaert, 1982; Han & Tian, 2018a, 2020). $\frac{E}{E_{Pen}}$ is then expressed as a function of the atmospheric wetness index $\frac{E_{rad}}{E_{Pen}}$ by considering that the change in $\frac{E_{rad}}{E_{Pen}}$ can be completely induced by the change in land surface wetness (Han & Tian, 2018a). However, the land surface wetness and atmospheric wetness are not necessarily fully coupled. Advections from the outside (Brutsaert & Stricker, 1979) or large-scale synoptic changes (Liu et al., 2011; Shuttleworth et al., 2009) may play important roles in determining the near-surface atmospheric variables above a natural landscape.

Taking the wet surfaces investigated in this study as the extremes, the assumption of the traditional complementary principle does not hold because the water availability is ample and changeless. However, $\frac{E_{rad}}{E_{Pen}}$ varies significantly due to advections or large-scale synoptic changes, and $\frac{E}{E_{Pen}}$ is still highly related to $\frac{E_{rad}}{E_{Pen}}$, which can be described by the SGC equation. The results imply that $\frac{E}{E_{Pen}}$ can be expressed as a function of $\frac{E_{rad}}{E_{Pen}}$ regardless whether its changes come from the land surface (changes in water availability) or the atmospheric aspects (advections or large-scale synoptic changes).

For the open surfaces shown in former sections, the growth of $\frac{E}{E_{Pen}}$ on $\frac{E_{rad}}{E_{Pen}}$ exhibits nonlinear characteristics with decreasing growth rate for large values of $\frac{E_{rad}}{E_{Pen}}$, which is also shown over natural land surfaces (Han & Tian, 2018a). This upper flatness feature requires that E and E_{aero} increase with constant E_{rad} when $\frac{E}{E_{Pen}}$

decreases from one (Han & Tian, 2018a, 2019). If E_{rad} is constant, an increase in E_{aero} indicates an increase in the vapor pressure deficit if the wind speed is changeless. However, the assumption of the complementary principle indicates that the vapor pressure deficit can only increase if less water was evaporated into the air, which means E will decrease. Thus, the upper flatness feature of the growth of $\frac{E}{E_{Pen}}$ upon $\frac{E_{rad}}{E_{Pen}}$ was questioned by considering that the change in E and E_{aero} in the same direction over a nearly wet surface is impossible (Szilagyi & Crago, 2019). However, the same direction changes in E and E_{aero} can be understood by considering the second type processes related to advections or large-scale synoptic changes. For example, the horizontal advection of hot dry air to the wet surface enhances E and E_{aero} with constant E_{rad} . Thus, the growth of $\frac{E}{E_{Pen}}$ on $\frac{E_{rad}}{E_{Pen}}$ is slow with large values of $\frac{E_{rad}}{E_{Pen}}$, which can explain the upper flatness feature.

For a natural landscape, the two above processes simultaneously exist, thereby explaining why the points of $\frac{E}{E_{Pen}}$ on $\frac{E_{rad}}{E_{Pen}}$ at the land site DS are scattered. The land site DS would be affected by the processes dominated at the lake sites, or advections from the lake considerably because the nearest distance to the shore is only 2 km. This condition can be detected because the daily E_{aero} at DS is highly correlated with the lake site PTS ($y=0.75x+0.29$, $R^2=0.69$ during 2014). However, the relative importance of the two processes varies with the surface wetness. Under water-limited conditions, the actual evaporation and potential evaporation are tightly linked via the surface, whereas the regional or large-scale advection would play a greater role than the landscape-scale processes under energy-limited conditions (Lintner et al., 2015). The complementary principle can be further generalized to cover the later processes. Thus, its capability to estimate evaporation over various types of land surface can be enhanced.

7 Summary

- (1) The meta-analysis based on the published results indicates seasonal variations of the PT coefficient, which are low in warm seasons but high in cold seasons. We confirmed this nonlinear feature of the dependence of E on E_{rad} over the wet surface and attributed it to the variations of E_{aero} by using the data over lakes and ocean.

- (2) The SGC equation, as a nonlinear modification of the linear AA approach for natural evaporating surfaces based on the complementary principle, can be extended to wet surfaces by setting its symmetric parameter to infinity. The wet surface SGC equation can effectively describe the nonlinear growth of E on E_{rad} over wet surfaces by including the influences of E_{aero} . The wet surface SGC equation with one calibrated parameter outperforms the linear PT equation for estimating evaporation because it considers the varying PT coefficient.
- (3) The parameter of the wet surface SGC equation may be related to the advections from the outside or the large-scale synoptic changes. The complementary principle can be further extended to include these processes.

Acknowledgments

This research was partially sponsored by the National Natural Science Foundation of China (No. 51579249, 51825902) and the Research Fund (No. 2020ZY06) of State Key Laboratory of Simulation and Regulation of Water Cycle in River Basin, China Institute of Water Resources and Hydropower Research.

Data of the Taihu Eddy Flux Network is available at <http://yncenter.sites.yale.edu>. Data of the the OAFlux project is available at <http://oafux.whoi.edu>. The data of the Winous Point Marsh site (WPT), Haibei alpine swamp site (HBW) and the Twitchell rice paddy site (TWT) are available at <https://fluxnet.org/data/fluxnet2015-dataset>. The data of the Mase paddy site (MSE) is available at http://asiaflux.net/index.php?page_id=83.

References

- Allen, R. G., Pereira, L. S., Raes, D., & Smith, M. (1998). *Crop evapotranspiration: Guidelines for computing crop water requirements*. FAO irrigation and drainage paper No. 56. Rome, Italy: Food and Agricultural Organization of the U.N. .
- Assouline, S., Li, D., Tyler, S., Tanny, J., Cohen, S., Bou-Zeid, E., . . . Katul, G. G. (2016). On the variability of the Priestley-Taylor coefficient over water bodies. *Water Resources Research*, 52(1), 150-163. doi:10.1002/2015wr017504
- Baldocchi, D., Knox, S., Dronova, I., Verfaillie, J., Oikawa, P., Sturtevant, C., . . . Detto, M. (2016). The impact of expanding flooded land area on the annual evaporation of rice. *Agricultural And Forest Meteorology*, 223, 181-193. doi:10.1016/j.agrformet.2016.04.001
- Bouchet, R. (1963). Evapotranspiration réelle et potentielle, signification climatique. *International Association of Hydrological Sciences Publication*, 62, 134-142.
- Brutsaert, W. (1982). *Evaporation into the Atmosphere: Theory, History, and Applications*. D. Reidel-Kluwer, Hingham.
- Brutsaert, W. (2005). *Hydrology: An Introduction*. New York: Cambridge Univ. Press.
- Brutsaert, W. (2015). A generalized complementary principle with physical constraints

- for land-surface evaporation. *Water Resources Research*, 51(10), 8087–8093, doi:8010.1002/2015WR017720. doi:10.1002/2015wr017720
- Brutsaert, W., Li, W., Takahashi, A., Hiyama, T., Zhang, L., & Liu, W. (2017). Nonlinear advection-aridity method for landscape evaporation and its application during the growing season in the southern Loess Plateau of the Yellow River basin. *Water Resources Research*, 53, 270–282.
- Brutsaert, W., & Parlange, M. B. (1998). Hydrologic Cycle explains the evaporation paradox. *Nature*, 396, 30.
- Brutsaert, W., & Stricker, H. (1979). An advection-aridity approach to estimate actual regional evapotranspiration. *Water Resources Research*, 15(2), 443–450.
- Budyko, M. I. (1974). *Climate and Life*: Academic presss, San Diego, Calif.
- Chu, H., Chen, J., Gottgens, J. F., Ouyang, Z., John, R., Czajkowski, K., & Becker, R. (2014). Net ecosystem methane and carbon dioxide exchanges in a Lake Erie coastal marsh and a nearby cropland. *Journal of Geophysical Research: Biogeosciences*, 119(5), 722–740.
- Chu, H., Gottgens, J. F., Chen, J., Sun, G., Desai, A. R., Ouyang, Z., . . . Czajkowski, K. (2015). Climatic variability, hydrologic anomaly, and methane emission can turn productive freshwater marshes into net carbon sources. *Glob Chang Biol*, 21(3), 1165–1181. doi:10.1111/gcb.12760
- De Bruin, H. A. R. (1978). A Simple Model for Shallow Lake Evaporation. *Journal Of Applied Meteorology*, 17(8), 1132–1134.
- De Bruin, H. A. R., & Keijman, J. Q. (1979). The Priestley-Taylor Evaporation Model Applied to a Large, Shallow Lake in the Netherlands. *Journal Of Applied Meteorology*, 18(7), 898–903.
- Eagleson, P. S. (2002). *Ecohydrology: Darwinian expression of vegetation form and function*. Cambridge: Cambridge University Press.
- Eichinger, W. E., Parlange, M. B., & Stricker, H. (1996). On the concept of equilibrium evaporation and the value of the Priestley-Taylor coefficient. *Water Resources Research*, 32(1), 161–164.
- Friedrich, K., Grossman, R. L., Huntington, J., Blanken, P. D., Lenters, J., Holman, K. D., . . . Kowalski, T. (2018). Reservoir Evaporation in the Western United States: Current Science, Challenges, and Future Needs. *Bulletin Of The American Meteorological Society*, 99(1), 167–187. doi:10.1175/bams-d-15-00224.1
- Granger, R. J. (1989). An examination of the concept of potential evaporation. *Journal Of Hydrology*, 111, 9–19. Retrieved from
- Guo, X., Liu, H., & Yang, K. (2015). On the Application of the Priestley–Taylor Relation on Sub-daily Time Scales. *Boundary-Layer Meteorology*, 156(3), 489–499. doi:10.1007/s10546-015-0031-y
- Han, S., Hu, H., & Tian, F. (2012). A nonlinear function approach for the normalized complementary relationship evaporation model. *Hydrological Processes*, 26(26), 3973–3981.
- Han, S., & Tian, F. (2018a). Derivation of a sigmoid generalized complementary function for evaporation with physical constraints. *Water Resources Research*, 54(7), 5050–5068. doi:doi: 10.1029/2017WR021755
- Han, S., & Tian, F. (2018b). Integration of Penman approach with complementary principle for evaporation research. *Hydrological Processes*, 32(19), 3051–3058.
- Han, S., & Tian, F. (2019). Reply to Comment by J. Szilagyi and R. Crago on “Derivation of a sigmoid generalized complementary function for evaporation with physical constraints”. *Water Resources Research*, 55(2), 1734–1736. doi:10.1029/2018WR023844

- Han, S., & Tian, F. (2020). A review of the complementary principle of evaporation: from the original linear relationship to generalized nonlinear functions. *Hydrology And Earth System Sciences*, 24(5), 2269-2285. doi:10.5194/hess-24-2269-2020
- Jury, W., & Tanner, C. (1975). Advection modification of the Priestley and Taylor evapotranspiration formula. *Agronomy Journal*, 67(6), 840-842.
- Katul, G. G., & Parlange, M. B. (1992). A Penman-Brutsaert Model for wet surface evaporation. *Water Resources Research*, 28(1), 121-126.
- Knox, S. H., Matthes, J. H., Sturtevant, C., Oikawa, P. Y., Verfaillie, J., & Baldocchi, D. (2016). Biophysical controls on interannual variability in ecosystem-scale CO₂ and CH₄ exchange in a California rice paddy. *Journal of Geophysical Research: Biogeosciences*, 121(3), 978-1001. doi:10.1002/2015jg003247
- Lee, X., Liu, S., Xiao, W., Wang, W., Gao, Z., Cao, C., . . . Wang, Y. (2014). The Taihu Eddy Flux Network: an observational program on energy, water and greenhouse gas fluxes of a large freshwater lake. *Bulletin Of The American Meteorological Society*, 95, 140530112919008.
- Li, L., & Yu, Q. (2007). Quantifying the effects of advection on canopy energy budgets and water use efficiency in an irrigated wheat field in the North China Plain. *Agricultural Water Management*, 89(1-2), 116-122. doi:10.1016/j.agwat.2006.12.003
- Li, X. Y., Ma, Y. J., Huang, Y. M., Hu, X., Wu, X. C., Wang, P., . . . Jiang, Z. Y. (2016). Evaporation and surface energy budget over the largest high-altitude saline lake on the Qinghai-Tibet Plateau. *Journal of Geophysical Research Atmospheres*, 121, 10470-10485. doi:doi:10.1002/2016JD025027
- Li, Z., Yu, G., Xiao, X., Li, Y., Zhao, X., Ren, C., . . . Fu, Y. (2007). Modeling gross primary production of alpine ecosystems in the Tibetan Plateau using MODIS images and climate data. *Remote Sensing Of Environment*, 107(3), 510-519. doi:10.1016/j.rse.2006.10.003
- Lintner, B., Gentile, P., Findell, K., & Salvucci, G. (2015). The Budyko and complementary relationships in an idealized model of large-scale land-atmosphere coupling. *Hydrology And Earth System Sciences*, 19(5), 2119-2131.
- Liu, H., Blanken, P. D., Weidinger, T., Nordbo, A., & Vesala, T. (2011). Variability in cold front activities modulating cool-season evaporation from a southern inland water in the USA. *Environmental Research Letters*, 6(2), 024022. doi:10.1088/1748-9326/6/2/024022
- McMahon, T., Peel, M., Lowe, L., Srikanthan, R., & McVicar, T. (2013). Estimating actual, potential, reference crop and pan evaporation using standard meteorological data: a pragmatic synthesis. *Hydrology And Earth System Sciences*, 17(4), 1331-1363.
- Morton, F. I. (1983). Operational estimates of areal evapotranspiration and their significance to the science and practice of hydrology. *Journal Of Hydrology*, 66, 1-76.
- Parlange, M. B., & Katul, G. G. (1992). Estimation of the diurnal variation of potential evaporation from a wet bare soil surface. *Journal Of Hydrology*, 132, 71-89.
- Penman, H. L. (1948). Natural Evaporation from open water, bare soil and grass. *Proceedings of the Royal Society of London, Series A, Mathematical and Physical Sciences*, 193, 120-145.
- Priestley, C. H., & Taylor, R. J. (1972). On the assessment of surface heat flux and evaporation using large-scale parameters. *Monthly Weather Review*, 100, 81-92.
- Roderick, M. L., & Farquhar, G. D. (2002). The cause of decreased pan evaporation

791 over the past 50 years. *Science*, 298, 1410-1411.

792 Saito, M., Miyata, A., Nagai, H., & Yamada, T. (2005). Seasonal variation of carbon
793 dioxide exchange in rice paddy field in Japan. *Agricultural And Forest*
794 *Meteorology*, 135(1-4), 93-109. doi:10.1016/j.agrformet.2005.10.007

795 Shuttleworth, W. J., & Calder, I. R. (1979). Has the Priestley-Talyor equation any
796 relevance to forest evaporation. *J. Appl. Meteorol*, 18, 639-646.

797 Shuttleworth, W. J., Serrat-Capdevila, A., Roderick, M. L., & Scott, R. L. (2009). On
798 the theory relating changes in area-average and pan evaporation. *Quarterly*
799 *Journal Of The Royal Meteorological Society*, 135, 1230-1247.

800 Slatyer, R. O., & McIlroy, I. C. (1961). *Practical Micrometeorology*. Melbourne,
801 Australia: CSIRO.

802 Szilagyi, J., & Crago, R. (2019). Comment on “Derivation of a sigmoid generalized
803 complementary function for evaporation with physical constraints” by S. Han
804 and F. Tian. *Water Resources Research*, 55, 868–869.

805 Twine, T. E., Kustas, W. P., Norman, J. M., Cook, D. R., Houser, P. R., Meyers, T. P., . . .
806 Wesely, M. L. (2000). Correcting eddy-covariance flux underestimates over a
807 grassland. *Agricultural & Forest Meteorology*, 103(3), 279-300.

808 Wang, J., Song, C., Reager, J. T., Yao, F., Famiglietti, J. S., Sheng, Y., . . . Wada, Y.
809 (2018a). Recent global decline in endorheic basin water storages. *Nature*
810 *Geoscience*, 11, 926-932. doi:10.1038/s41561-018-0265-7

811 Wang, L., Tian, F., Han, S., & Wei, Z. (2020). Determinants of the asymmetric
812 parameter in the complementary principle of evaporation. *submitted to Water*
813 *Resources Research*, 2019WR026570.

814 Wang, W., Lee, X., Xiao, W., Liu, S., Schultz, N., Wang, Y., . . . Zhao, L. (2018b).
815 Global lake evaporation accelerated by changes in surface energy allocation in
816 a warmer climate. *Nature Geoscience*. doi:10.1038/s41561-018-0114-8

817 Wang, W., Xiao, W., Cao, C., Gao, Z., Hu, Z., Liu, S., . . . Lee, X. (2014). Temporal and
818 spatial variations in radiation and energy balance across a large freshwater lake
819 in China. *Journal Of Hydrology*, 511, 811-824.
820 doi:10.1016/j.jhydrol.2014.02.012

821 Winter, T. C., Rosenberry, D. O., & Sturrock, A. M. (1995). Evaluation of 11 Equations
822 for Determining Evaporation for a Small Lake in the North Central United
823 States. *Water Resources Research*, 31(4), 983–993.

824 Yang, Y., & Roderick, M. L. (2019). Radiation, surface temperature and evaporation
825 over wet surfaces. *Quarterly Journal Of The Royal Meteorological Society*,
826 145(720), 1118-1129. doi:10.1002/qj.3481

827 Yu, G.-R., Wen, X.-F., Sun, X.-M., Tanner, B. D., Lee, X., & Chen, J.-Y. (2006).
828 Overview of ChinaFLUX and evaluation of its eddy covariance measurement.
829 *Agricultural And Forest Meteorology*, 137(3-4), 125-137.
830 doi:10.1016/j.agrformet.2006.02.011

831 Yu, L., & Weller, R. A. (2007). Objectively Analyzed Air–Sea Heat Fluxes for the
832 Global Ice-Free Oceans (1981–2005). *Bulletin Of The American Meteorological*
833 *Society*, 88(4), 527-540. doi:10.1175/bams-88-4-527

834 Zhang, L., Cheng, L., & Brutsaert, W. (2017). Estimation of land surface evaporation
835 using a generalized nonlinear complementary relationship. *Journal of*
836 *Geophysical Research: Atmospheres*, 122(3), 1475-1487.
837 doi:10.1002/2016jd025936

838 Zhang, Q., & Liu, H. (2013). Interannual variability in the surface energy budget and
839 evaporation over a large southern inland water in the United States. *Journal of*
840 *Geophysical Research: Atmospheres*, 118(10), 4290-4302.

841 doi:10.1002/jgrd.50435
842 Zhao, G., & Gao, H. (2019). Estimating reservoir evaporation losses for the United
843 States: Fusing remote sensing and modeling approaches. *Remote Sensing Of*
844 *Environment*, 226, 109-124. doi:10.1016/j.rse.2019.03.015
845 Zhou, H., Han, S., & Liu, W. (2020). Evaluation of two generalized complementary
846 functions for annual evaporation estimation on the Loess plateau, China.
847 *Journal Of Hydrology*, 587, 124980. doi:doi: 10.1016/j.jhydrol.2020.124980
848